Analytical Modeling of Capacitances for GaN HEMTs, Including Parasitic Components

Aixi Zhang, *Student Member, IEEE*, Lining Zhang, *Member, IEEE*, Zhikai Tang, *Student Member, IEEE*, Xiaoxu Cheng, Yan Wang, Kevin J. Chen, *Fellow, IEEE*, and Mansun Chan, *Fellow, IEEE*

***Abstract*— In this paper, a surface potential-based terminal charge and capacitance model, including parasitic components for AlGaN/GaN HEMTs is developed. First, by solving the charge control equations, the sheet charge density in the channel is modeled with a close-form expression. Then, using this result, based on the surface potential definition, the intrinsic terminal charges and capacitances are derived consistently with current model. Finally, by introducing parasitic components, the capacitances for the full structure of the HEMT devices are given. The model is evaluated step-by-step with good agreements compared with the TCAD simulations and the experimental data. Meanwhile, the effects of bulk traps and surface traps in the capacitances are analyzed. The complete model, including currents and capacitances has been implemented in *i*-MOS platform for evaluations and circuit simulations.**

***Index Terms*— Capacitance model, parasitic capacitance, sheet charge, surface potential, terminal charge, trap.**

I. Introduction

AlGaN/GaN HEMTs have been widely studied in recent years because of the promising performance for radio frequency/microwave power amplifiers and high-power switching applications [1], [2]. Along with the fast development of GaN-based device technology and circuit integration, reliable predictive models are of great value for circuit design and simulation. For the electric current model, the research has evolved along the path from empirical models [3], [4] to threshold voltage-based analytical models [5], [6] to surface potential-based physical models [7], [8]. However, the capacitance-voltage (C–V) characteristics, which are equally important for circuit simulation, have received less attention. Lee and Webb [9] reported an empirical fitting model, which features a large number of unphysical fitting parameters. Recently, Khandelwal *et al.* [10], [11] presented their work on an intrinsic, surface potential-based capacitance model. The parasitic capacitance components in GaN HEMTs are not considered in their model.

Manuscript received November 12, 2013; revised January 1, 2014; accepted January 2, 2014. Date of publication January 17, 2014; date of current version February 20, 2014. This work was supported by Hong Kong's University Grant Committee under the Area of Excellence Project AoE-P04-08. The review of this paper was arranged by Editor G. Ghione.

A. Zhang, L. Zhang, Z. Tang, K. J. Chen, and M. Chan are with the Department of Electronic and Computer Engineering, Hong Kong University of Science and Technology, Hong Kong (e-mail: zhangaixi2008@gmail.com; lnzhang@ust.hk; zhikaitang@ust.hk; eekjchen@ust.hk; mchan@ust.hk).

X. Cheng and Y. Wang are with the Institute of Microelectronics, Tsinghua University, Beijing 100084, China (e-mail: chengxx85@gmail.com; wangy46@tsinghua.edu.cn).

Color versions of one or more of the figures in this paper are available online at http://ieeexplore.ieee.org.

Digital Object Identifier 10.1109/TED.2014.2298255

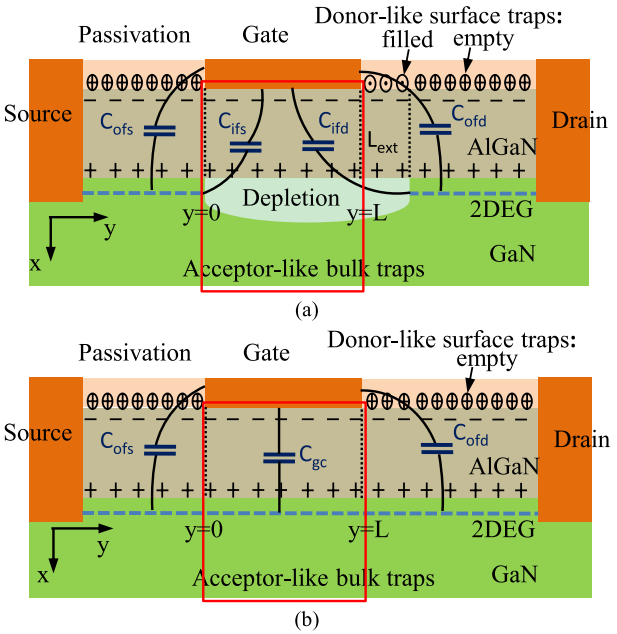

Fig. 1. Cross-sectional schematics of an AlGaN/GaN HEMT and its capacitance partition, including the intrinsic capacitance and inner fringing and outer fringing capacitances of (a) off-state and (b) on-state. The donor-like surface traps and acceptor-like bulk traps are sketched. The core parts of the devices are highlighted by the red boxes. The extended length L_{ext} accounts for the extended depletion region induced by the electrons injection to the surface traps [20], [21], which affects fringing capacitances.

Fig. 1 shows the capacitance schematics for an AlGaN/GaN HEMT with donor-like surface traps and acceptor-like bulk traps at both OFF-state and ON-state. The intrinsic capacitance C_{gc} is formed between the gate and channel 2-dimensional electron gas (DEG), which is induced by the polarization effect. The TCAD simulations [12] show that the parasitic (fringing) capacitances C_{if} and C_{of} due to the inner and outer fringing electric fields account for $>10\%$ in the total capacitances, therefore, they also need to be considered.

In this paper, an analytical capacitance model is developed, including the parasitic components. The intrinsic charge and capacitance model is developed based on the precise calculation of sheet charge density and surface potential. The fringing capacitances are included by unified conformal mapping method. The model is verified with extensive TCAD simulations. The effects of the bulk traps and surface traps are

TABLE I
SYMBOLS DEFINITION

Symbols	Definitions
n_s	The sheet charge density (density of 2DEG)
V_c	The channel potential
ε_{AlGaN}	The permittivity of AlGaN
ε_{SiN}	The permittivity of SiN (passivation material)
$d\,(T_{AlGaN})$	The thickness of the AlGaN layer
q	The electron charge
E_F	The Fermi level relative to the bottom of the conduction band
u_i	Position of E_i determined by Robin boundary condition [15]
D	The conduction band density of states of a 2D system
k	The Boltazmann's constant
T	The ambient temperature
ϕ_t	The thermal voltage, $\phi_t = kT/q$
ϕ_{ss}	Surface potential at source side where $V_c = V_s$
ϕ_{sd}	Surface potential at drain side where $V_c = V_{ds}$
$\Delta\phi$	Difference between two channel sides $\Delta\phi = \phi_{sd} - \phi_{ss}$
ϕ_{sm}	Mid-value of surface potential $\phi_{sm} = (\phi_{ss} + \phi_{sd})/2$
s	Difference of surface potential to mid-value $s = \phi_s - \phi_{sm}$
q_i	Normalized channel electron density $q_i = qn_s / C_{ox} = q_{im} - s$
q_{im}	q_i at ϕ_{sm}, i.e., $q_{im} = V_{gs} - V_{OFF} - \phi_{sm}$
E_{sat}	The saturation electric field

analyzed as well. Finally, the full model is verified by experimental data. The capacitance model and the current model have been implemented into the *i*-MOS platform [13], which also supports circuit simulations. This paper is organized as follows. The derivations of the models are demonstrated in Section II. The models are verified and analyzed in Section III. Finally, this paper is concluded in Section IV.

II. INTRINSIC AND FRINGING CAPACITANCE MODEL

In this section, the sheet charge density is solved with a close-form expression. Using this result, based on the surface potential definition, the model of intrinsic capacitances is developed. The model of fringing capacitances is also given. The symbols used in this section are listed in Table I.

A. Derivation of Sheet Charge Density

The well-known charge control equations as self-consistent solution of Poisson's equation and Schrödinger's equations in the quantum well are expressed as [14]

$$n_s = \frac{\varepsilon_{\mathrm{AlGaN}}}{qd}(V_{\mathrm{gs}} - V_c - V_{\mathrm{OFF}} - E_F) \tag{1}$$

$$E_i = u_i n_s^{2/3} \tag{2}$$

$$n_s = \sum_{i=0}^{\infty} DkT \ln\left[1 + \exp\left(\frac{E_F - E_i}{\phi_t}\right)\right]. \tag{3}$$

In the following calculation, only the fundamental sub-band energy level E_0 is considered since the electrons contributed by other bands can be neglected [8]. With the denotations of $V_{\mathrm{go}} = V_{\mathrm{gs}} - V_c - V_{\mathrm{OFF}}$, from (1)–(3), the equation of Fermi level E_F is expressed as

$$V_{\mathrm{go}} - E_F = \frac{qDkTd}{\varepsilon_{\mathrm{AlGaN}}} \ln \times\left[1 + \exp\left(\frac{E_F}{\phi_t} - \frac{u_0}{\phi_t}\left[\frac{\varepsilon_{\mathrm{AlGaN}}}{qd}(V_{\mathrm{go}} - E_F)\right]^{\frac{2}{3}}\right)\right]. \tag{4}$$

The difficulty to solve it is that E_F is an implicit function of the gate voltage V_{gs} and the channel potential V_c. The solution used here is to give an initial solution first and then use a correction term for refinement [8]. After three times refinement, the absolute error of the E_F reaches under 1 fV with extensive validations compared with the numerical solutions, which only consider the fundamental level in the 2-DEG channel, E_0. Then, the sheet charge density n_s can be calculated accurately from (1).

B. Intrinsic Charge and Capacitance Model

Using the sheet charge density model, the intrinsic charge and capacitances can be derived based on the surface potential, which is $\phi_s = V_c + E_F$ defined as the bottom of conduction band [8].

A typical surface potential based drift-diffusion model for drain current is given as [16]

$$I_{\mathrm{ds}} = \mu \mathrm{WC_{ox}}(q_{\mathrm{im}} - s + \phi_t)ds/dy. \tag{5}$$

Considering the electric field along channel $E_y = ds/dy$ and the velocity model $v = \mu_0 E_y/(1 + aE_y/E_{\mathrm{sat}})$ [6], (5) can be written as

$$I_{\mathrm{ds}} = \mu_0 \mathrm{WC_{ox}} \frac{(q_{\mathrm{im}} - s + \phi_t)ds/dy}{1 + aE_y/E_{\mathrm{sat}}}. \tag{6}$$

By integrating (6) along the channel from $y = 0$ to $y = L$, the current is given as

$$I_{\mathrm{ds}} = \mu_0 \frac{W}{L} C_{\mathrm{ox}} \frac{(q_{\mathrm{im}} + \phi_t)\Delta\phi}{G_{\mathrm{vsat}}} \tag{7}$$

where $G_{\mathrm{vsat}} = 1 + a\sqrt{\Delta\phi^2 + \delta}/(E_{\mathrm{sat}}L)$ is used instead of $1 + a\Delta\phi/(E_{\mathrm{sat}}L)$ to fulfill the Gummel symmetry test [17].

Since the drain current is independent with position, by substituting (7) into (6) and denoting the symbol $H = G_{\mathrm{vsat}}/(q_{\mathrm{im}} + \phi_t)$, the relation between the surface potential and the position is given as [18]

$$\frac{dy}{\mathrm{ds}} = (1 - sH)\frac{L}{\Delta\phi}. \tag{8}$$

Using (8), the gate charge is derived as

$$Q_g = \mathrm{WC_{ox}} \int_0^L q_i \mathrm{dy} = \mathrm{WLC_{ox}}\left(V_{\mathrm{go}} - \phi_{\mathrm{sm}} + H\Delta\phi^2/12\right). \tag{9}$$

Using Ward–Dutton charge partition method [19], the drain charge is expressed as

$$Q_d = -\mathrm{WC_{ox}} \int_0^L \frac{y}{L} q_i dy = -\mathrm{WLC_{ox}}\left[\frac{q_{\mathrm{im}}}{2} - \frac{\Delta\phi}{12}\left(1 - \frac{H\Delta\phi}{2} - \frac{H^2\Delta\phi^2}{20}\right)\right]. \tag{10}$$

To consider the channel length modulation effect, the length of the velocity-saturation region is given as [5]

$$\Delta L = p \sinh^{-1}\left(\frac{V_{\rm ds} - V_{\rm dse}}{pE_{\rm sat}}\right) \tag{11}$$

where p is a fitting parameter and $V_{\rm dse}$ is the potential at the end of the gradual channel region given as

$$V_{\rm dse} = V_{\rm ds}/\left[1 + (V_{\rm ds}/V_{\rm dsat})^m\right]^{1/m}. \tag{12}$$

Now the factor $\gamma_L = 1/(1 + \Delta L/L)$ is introduced to improve the continuity of the model, then the effective channel length $L_{\rm eff} = \gamma_L L$ is used in (7) to improve the current model. In addition, the gate charge and the drain charge models are modified as

$$Q_g = {\rm WLC_{ox}}\left[\gamma_L\left(V_{\rm go} - \phi_{\rm sm} + H\Delta\phi^2/12\right) + (1-\gamma_L)q_{\rm id}\right] \tag{13}$$

$$Q_d = -{\rm WLC_{ox}}\left\{\gamma_L\left[\frac{q_{\rm im}}{2} - \frac{\Delta\phi}{12}\left(1 - \frac{H\Delta\phi}{2} - \frac{H^2\Delta\phi^2}{20}\right)\right] + (1-\gamma_L)q_{\rm id}\right\} \tag{14}$$

where $q_{\rm id}$ is the value of normalized channel electron density q_i at drain side. Then, the source charge is given as

$$Q_s = -Q_g - Q_d. \tag{15}$$

Finally, all the intrinsic terminal capacitances are given analytically by the following derivations, which are not given in detail here due to the complexity of the formulas

$$\begin{cases} C_{\rm gd} = -\partial Q_g/\partial V_{\rm ds} & C_{\rm gg} = \partial Q_g/\partial V_{\rm gs} & C_{\rm gs} = C_{\rm gg} - C_{\rm gd} \\ C_{\rm dd} = \partial Q_d/\partial V_{\rm ds} & C_{\rm dg} = -\partial Q_d/\partial V_{\rm gs} & C_{\rm ds} = C_{\rm dd} - C_{\rm dg} \\ C_{\rm sd} = -\partial Q_s/\partial V_{\rm ds} & C_{\rm sg} = -\partial Q_s/\partial V_{\rm gs} & C_{\rm ss} = C_{\rm sg} + C_{\rm sd}. \end{cases} \tag{16}$$

C. Parasitic (Fringing) Capacitance Model

The fringing capacitance is mainly formed due to the fringing electric field. As shown in Fig. 2, the electric field between the vertical sidewall of the gate and the horizontal surfaces of the 2-DEG in the access region accounts for the outer fringing capacitance $C_{\rm of}$, and the electric field between the horizontal sidewall of the gate and the vertical surfaces of the 2-DEG accounts for the inner fringing capacitance $C_{\rm if}$. The fringing electric field between the ends of terminals is shared by $C_{\rm of}$ and $C_{\rm if}$. The extended length $L_{\rm ext}$ accounts for the extended depletion region induced by the electrons injection to the donor-like surface traps [20], [21], as also shown in Fig. 1(a). $L_{\rm ext}$ is determined by the surface trap density and the terminal voltages, which will disappear when the device transfers from off-state to on-state. The maximum value of $L_{\rm ext}$ is given as a fitting parameter in this paper. The conformal mapping method is used here to model both the fringing components.

For the $C_{\rm of}$ model, since the electric field goes through the passivation layer and AlGaN layer, an effective dielectric constant is empirically described as

$$\varepsilon_x = \varepsilon_{\rm SiN}\left\{1 + \exp\left[-\frac{T_g}{T_{\rm AlGaN}}\frac{\varepsilon_{\rm AlGaN}}{\sqrt{(\varepsilon_{\rm AlGaN} - \varepsilon_{\rm SiN})^2 + \delta_2}}\right]\right\} \tag{17}$$

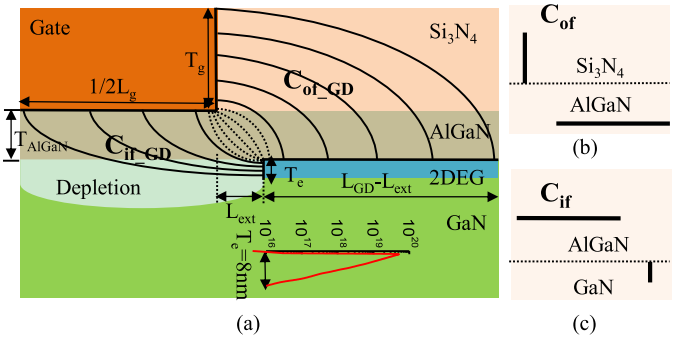

Fig. 2. (a) Cross-sectional schematic view for the inner and outer fringing capacitances modeling of the drain side by conformal mapping method. Solid lines: normal electric field between the side wall of the gate and the 2-DEG in the access region. Dashed lines: fringing electric field at the ends of the terminals. The charge density in the access region is also shown, which indicates the charge thickness T_e accounting for the inner fringing capacitance calculation can be used as 8 nm. (b) and (c) Used structures in COMSOL simulation to extract the outer fringing and inner fringing capacitances separately, where both the gate and 2-DEG are regarded as 1-D ideal metallic plates.

where δ_2 has a tiny positive value for SPICE convergence. Then, $C_{\rm of}$ is modeled by conformal mapping as follows [22]:

$$C_{\rm of} = \frac{2\varepsilon_x}{\pi}\ln\left(\frac{T_{\rm AlGaN} + \eta T_g + \sqrt{L_{\rm ext}^2 + (\eta T_g)^2 + 2T_{\rm AlGaN}\eta T_g}}{L_{\rm ext} + T_{\rm AlGaN}}\right) + \frac{k\varepsilon_{\rm AlGaN}}{\pi}\ln\left(\frac{\pi W}{\sqrt{L_{\rm ext}^2 + T_{\rm AlGaN}^2}}\right)\exp\left(-\left|\frac{L_{\rm ext} - T_{\rm AlGaN}}{L_{\rm ext} + T_{\rm AlGaN}}\right|\right) \tag{18}$$

where $\eta = \exp\left(L_{\rm gs/gd} + L_{\rm ext} - \sqrt{L_{\rm ext}^2 + T_g^2 + 2T_{\rm AlGaN}T_g}\big/\tau L_{\rm gs/gd}\right)$, and τ and k are fitting parameters. The first part of (18) accounts for the normal electric field and the second part accounts for the terminal fringing electric field.

For the $C_{\rm if}$ model, by only changing ε_x to $\varepsilon_{\rm AlGaN}$, T_g to T_e and $L_{\rm gs/gd}$ to $1/2L_g$, (18) is used to provide the maximum value $C_{\rm if\_max}$, which is the value in the off-state. Then, $C_{\rm if}$ will decrease and finally be screened by the channel electrons when the device turns from off-state to on-state. Therefore, the final $C_{\rm if}$ for source side and drain side is given as [23]

$$C_{\rm ifs/d} = C_{\rm if\_max}\exp\left(-\frac{V_{\rm gs} - V_{\rm off} - \phi_{s/d}}{\lambda\phi_t}\right) \tag{19}$$

where ϕ_s is the source side surface potential, ϕ_d is the drain side surface potential, and λ is a fitting parameter and given as 0.1 for a general case.

III. Capacitance Model Verification and Analyses

By the derived analytic model of the sheet charge density, terminal charges, and intrinsic and parasitic capacitances, all I–V and C–V characteristics of a GaN HEMT device can be predicted and analyzed with respect to different geometrical parameters and bias conditions. Here, the terminal charges and capacitances are focused on rather than I–V characteristics,

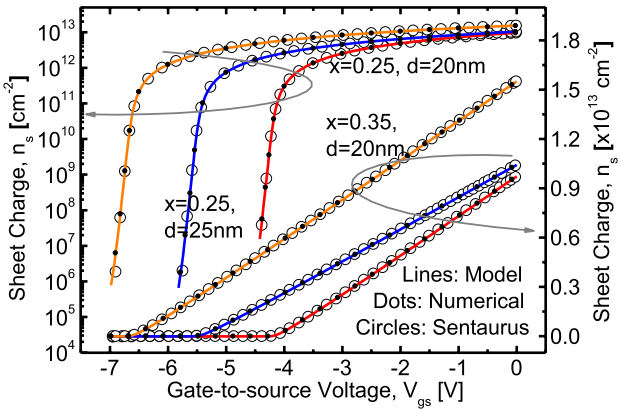

Fig. 3. Comparison of analytical models, TCAD simulations, and numerical results of sheet charge density versus gate voltage at $T = 300$ K. x is AlN mole fraction in AlGaN layer. The Schottky gate barrier height is $\Phi_B = 1.5$ eV. The TCAD data is extracted by $n_s = \varepsilon_{\rm GaN}(E_{x\_\rm top} - E_{x\_\rm bottom})/q$, where $E_{x\_\rm top}$ is the extracted maximum value of the vertical electric field in the central channel region of an extremely long channel device and $E_{x\_\rm bottom}$ is almost zero. The numerical results are obtained by solving the (1)–(3) iteratively.

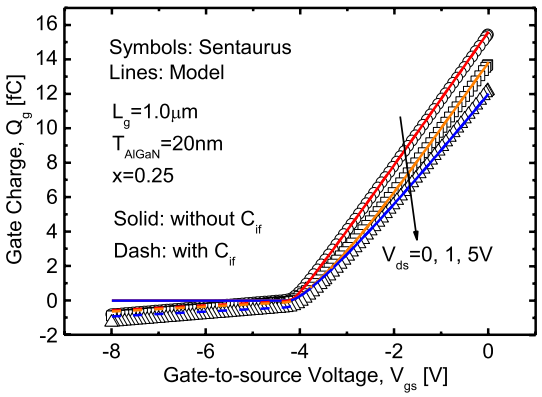

Fig. 4. Gate charge of the core part versus $V_{\rm gs}$ obtained from the proposed model and TCAD simulations. The deviation in the subthreshold region is due to inner fringing charge. $\Phi_B = 1.5$ eV.

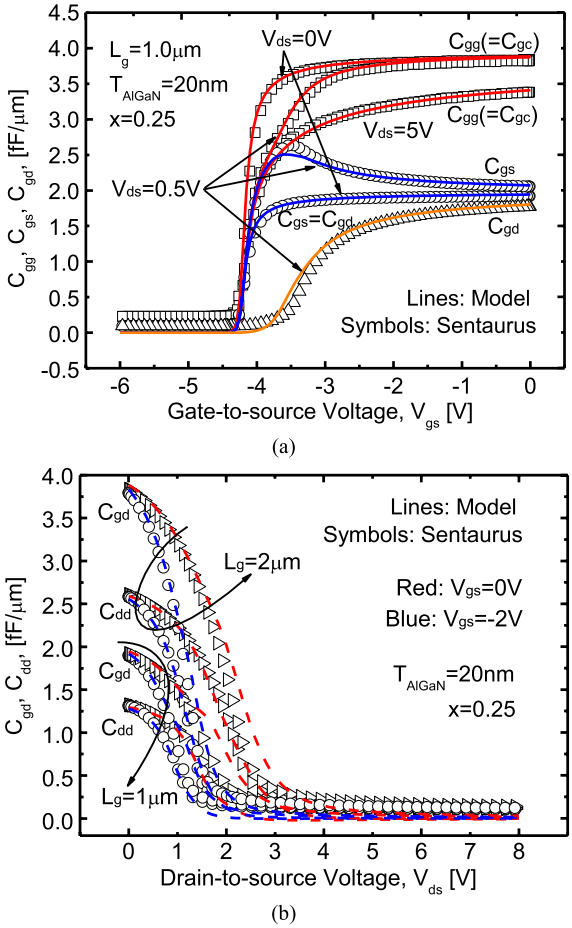

Fig. 5. Verification of intrinsic capacitances of the core model. (a) $C_{\rm gg}$, $C_{\rm gs}$, and $C_{\rm gd}$ versus $V_{\rm gs}$ with different $V_{\rm ds}$. (b) $C_{\rm dd}$ and $C_{\rm gd}$ versus $V_{\rm ds}$ with different $V_{\rm gs}$ and gate length L_g. $\Phi_B = 1.5$ eV.

which have been analyzed in [8]. In this section, the validity of the model is verified with extensive TCAD simulations from the sheet charge density to both the intrinsic and parasitic capacitances model. Finally, the full model is verified by experimental data.

The model of sheet charge density, which is normally known as the 2-DEG, is shown in Fig. 3 compared with both the TCAD simulations and the numerical results of (1)–(3). The TCAD simulations are used to extract the parameter u_0 in (3), which is given as 1.1312×10^{-12} V $\cdot$ m$^{4/3}$. Good agreements are achieved, which promises the feasibility of the terminal charge model.

To verify the core model, the core part of the HEMT device with source/drain contacts directly touching the 2-DEG at the gate edges, as highlighted in Fig. 1 by the red boxes, is used in the TCAD simulations. No bulk traps is distributed in the structure for simplicity. To eliminate the effect of outer fringing capacitance, the gate thickness is set to zero. The constant mobility model with high field saturation activated is used and the Fermi statistics is adopted. The Poisson equation and current continuity equations for electrons and holes are solved.

After verification of sheet charge density, the analytical gate charge Q_g versus $V_{\rm gs}$ with different $V_{\rm ds}$ conditions is shown in Fig. 4 compared with TCAD simulations. In the linear and saturation regions, the model shows good agreements. In the subthreshold region, the variation of the solid lines is due to the inner fringing charge, which is not included in this comparison.

Then, the intrinsic capacitances are verified with extensive TCAD simulations. In the simulations, the sinusoidal steady-state analysis [24] is used to get the impedance matrix of GaN HEMTs, including the terminal capacitances. In Fig. 5, the gate and drain capacitances and transcapacitances with different $V_{\rm gs}$, $V_{\rm ds}$, and gate length conditions are shown as examples. Good agreements are achieved, which indicates that, the model covers all the operating regions and works well with different gate lengths. In addition, the capacitance behaviors of the HEMTs predicted with the models are similar as MOSFETs. Again, the variation in the subthreshold region is due to the inner fringing capacitance.

For the parasitic components, the models of $C_{\rm if\_max}$ and $C_{\rm of}$ are verified separately by COMSOL simulations [25] as

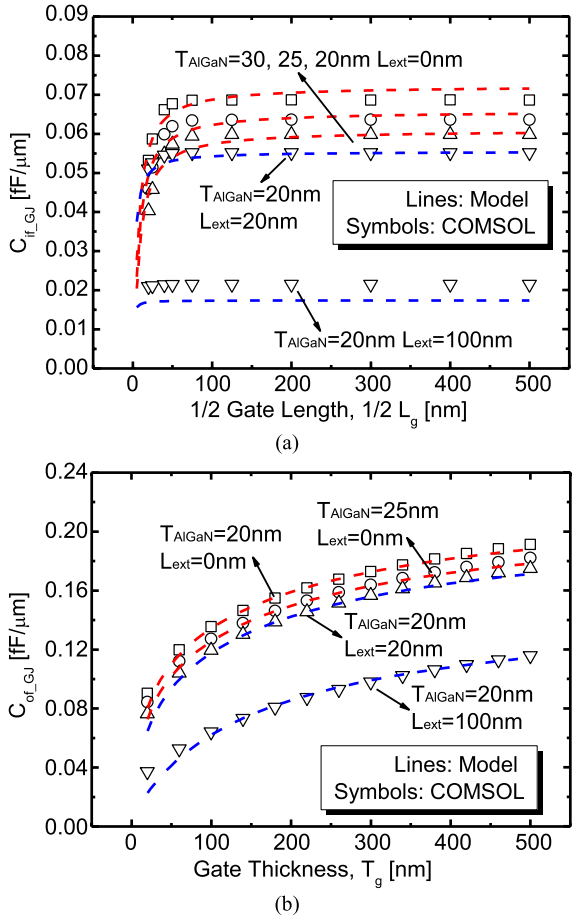

Fig. 6. Comparison of the model and TCAD simulations of (a) inner fringing capacitance versus 1/2 L_g and (b) outer fringing capacitance versus T_g with different geometries. J equals to S or D for the source side and drain side, respectively. $\tau = 1.5$ and $k = 0.18$ are the two fitting parameters.

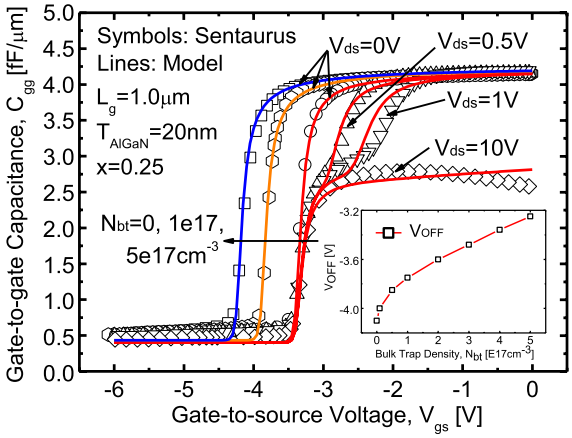

Fig. 7. Verification of C_{gg} versus V_{gs} under different V_{ds} conditions for full structure model compared with TCAD simulations. The parasitic capacitances are included. The effect of the acceptor-like bulk trap density (N_{bt}) is also analyzed by tuning the parameter of the offset voltage V_{OFF}, as shown in the inset. $T_g = 200$ nm. $L_{ext} = 20$ nm. $\Phi_B = 1.5$ eV.

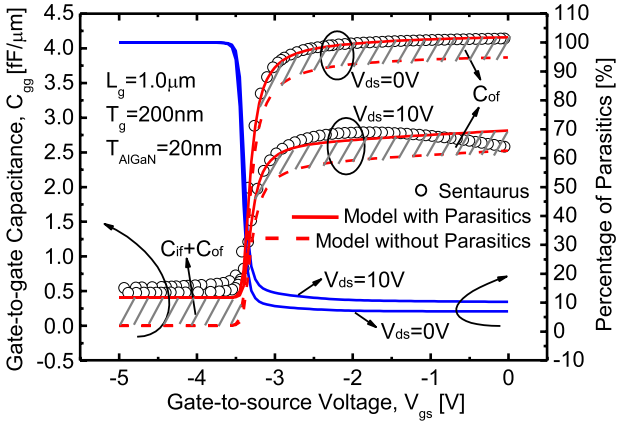

Fig. 8. Bias-dependent relative percentage of parasitics in the C_{gg}. The shadowed region accounts for the parasitics, which include both C_{of} and C_{if} in the off-state and only C_{of} in the on-state. $L_{gs} = 1$ μm. $L_{gd} = 2$ μm. $L_{ext} = 20$ nm.

shown in Fig. 6. The structures used to extract the outer fringing and inner fringing capacitances separately are given in Fig. 2(b) and (c), where both the gate and 2-DEG are regarded as 1-D ideal metallic plates. The models for these two capacitances are given by a same set of parameters and show good agreements. The effect of decreasing fringing capacitance with a larger L_{ext} induced by the surface traps is also shown and modeled well in this figure. The validity of the C_{if} model is also confirmed by the terminal charges Q_g shown with the dash lines in Fig. 4.

Finally, the real device with access regions, as shown in Fig. 1, is simulated. In the TCAD simulation, the acceptor-like bulk trap density is set as 5×10^{17} cm^{-3} in both GaN substrate and AlGaN layer, and the donor-like surface trap density is set as 3.5×10^{13} cm^{-2} distributed at the interface of AlGaN and SiN passivation. The polarization charge densities in both the GaN/AlGaN and the AlGaN/SiN interfaces, which are determined by the thickness of AlGaN layer and AlN mole fraction, are also included.

The capacitances, including the parasitic components are verified extensively with TCAD simulations, and Fig. 7 shows an example of C_{gg} versus V_{gs}. The traps set in the simulation also affect the capacitances. The acceptor-like bulk traps affect the capacitances by shifting the offset voltage V_{OFF}. The donor-like surface traps affect the parasitic capacitances through changing the L_{ext}, which is given as 20 nm here, and the value is similar as observed in the TCAD. The simulation can also reproduce the slight tendency of C_{gg} decreasing at high V_{ds}, which is a unique phenomenon widely reported in the HEMT devices [9], [26]. This feature is not yet included in the model, but the model still has reasonable accuracy in the saturation region.

Fig. 8 shows the percentage of parasitic capacitances in C_{gg} with the gate thickness as 200 nm, which is normally used in GaN HEMT fabrications. With this design parameter, the fringing capacitance cannot be neglected, which contributes all the capacitances in the subthreshold region, and provides $>10\%$ of the total capacitance in the saturation operating regions.

A fabricated HEMT with the similar structure and geometries [27] shown in Fig. 1 is used for on-wafer S-parameter measurement. The gate capacitances are extracted using an equivalent circuit model [28] and compared with the model.

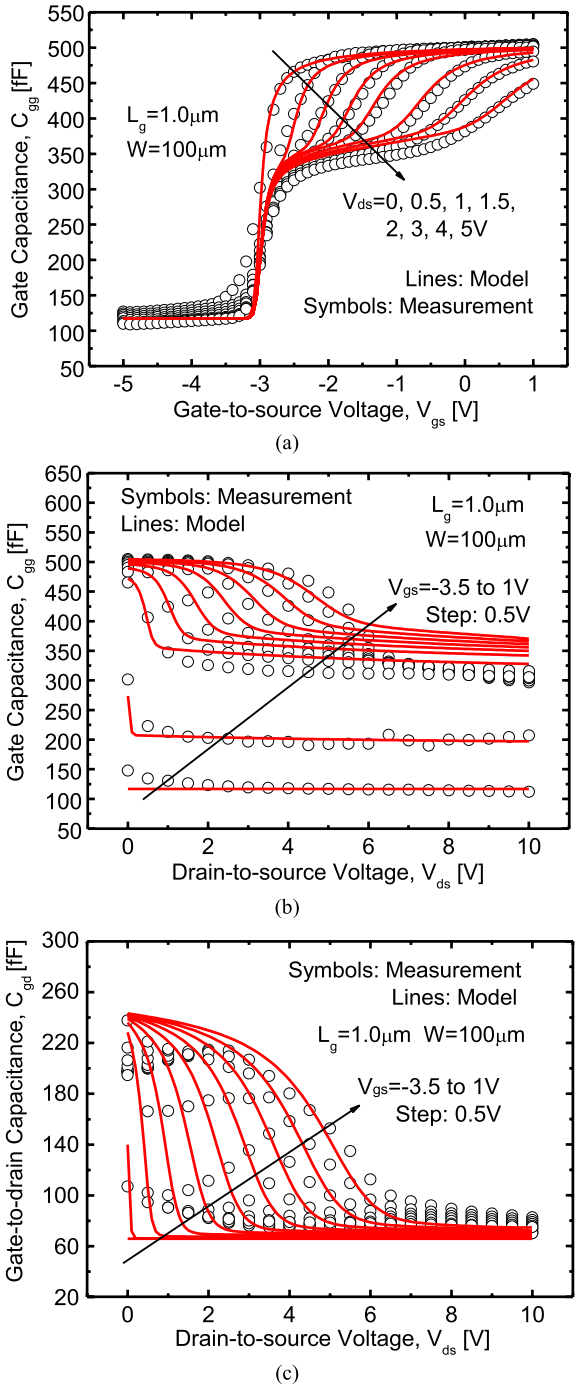

Fig. 9. Verification of (a) C_{gg} versus V_{gs} with different V_{ds}, (b) C_{gg} versus V_{ds} with different V_{gs}, and (c) C_{gd} versus V_{ds} with different V_{gs} compared with experimental data. The fringing capacitances are included in the comparisons.

Fig. 9 shows the examples of C_{gg} and C_{gd} measured and predicted by the model in all operation regions, and reasonably good agreements are obtained.

IV. Conclusion

A surface potential-based charge and capacitance model for AlGaN/GaN HEMTs is derived to give the three terminal charges and nine intrinsic transcapacitances, after the close-form modeling of sheet charge density. The parasitic components are also included with unified conformal mapping method and parameters. The effects of bulk traps and surface traps on the capacitances through changing the offset voltage and the extended gate length are also analyzed. The developed model covers all operation regions of the HEMTs and agrees well with the TCAD simulations and experimental data. The complete model, including current and capacitances, has been implemented into *i*-MOS platform, and it demonstrates a good validity to be used in GaN HEMT based circuit simulations.

References

[1] R. P. Smith, S. Sheppard, Y.-F. Wu, S. Heikman, S. Wood, W. Pribble, *et al.*, "AlGaN/GaN-on-SiC HEMT technology status," in *Proc. IEEE Compound Semicond. Integr. Circuits Symp.*, Oct. 2008, pp. 1–4.

[2] A. M. H. Kwan, X. Liu, and K. J. Chen, "Integrated gate-protected HEMTs and mixed-signal functional blocks for GaN smart power ICs," in *Proc. IEEE IEDM*, Dec. 2012, pp. 7.3.1–7.3.4.

[3] I. Angelov, K. Andersson, D. Schreurs, D. Xiao, N. Rorsman, V. Desmaris, *et al.*, "Large-signal modelling and comparison of AlGaN/GaN HEMTs and SiC MESFETs," in *Proc. APMC*, Yokohama, Japan, Dec. 2006, pp. 279–282.

[4] Agilent Technologies. Palo Alto, CA, USA. (2004, Aug.). *Agilent 85190A IC-CAP 2004: Nonlinear Device Models* [Online]. Available: http://cp.literature.agilent.com/litweb/pdf/iccap2004/pdf/icmdl.pdf

[5] M. Li and Y. Wang, "2-D analytical model for current–voltage characteristics and transconductance of AlGaN/GaN MODFETs," *IEEE Trans. Electron Devices*, vol. 55, no. 1, pp. 261–267, Jan. 2008.

[6] X. Cheng, M. Li, and Y. Wang, "Physics based compact model for AlGaN/GaN MODFET with closed form I–V and C–V characteristics," *IEEE Trans. Electron Devices*, vol. 56, no. 12, pp. 2881–2887, Dec. 2009.

[7] D. L. John, F. Allerstam, T. Rodle, S. K. Murad, and G. D. J. Smit, "A surface-potential based model for GaN HEMTs in RF power amplifier applications," in *Proc. IEEE IEDM*, Dec. 2010, pp. 8.3.1–8.3.4.

[8] X. Cheng and Y. Wang, "A surface-potential-based compact model for AlGaN/GaN MODFETs," *IEEE Trans. Electron Devices*, vol. 58, no. 2, pp. 448–454, Feb. 2011.

[9] J.-W. Lee and K. J. Webb, "A temperature-dependent nonlinear analytic model for AlGaN-GaN HEMT on SiC," *IEEE Trans. Microw. Theory Tech.*, vol. 52, no. 1, pp. 2–9, Jan. 2004.

[10] S. Khandelwal, Y. S. Chauhan, and T. A. Fjeldly, "Analytical modeling of surface-potential and intrinsic charges in AlGaN/GaN HEMT devices," *IEEE Trans. Electron Devices*, vol. 59, no. 10, pp. 2856–2860, Oct. 2012.

[11] S. Khandelwal, C. Yadav, S. Agnihotri, Y. S. Chauhan, A. Curutchet, T. Zimmer, *et al.*, "Robust surface-potential-based compact model for GaN HEMT IC design," *IEEE Trans. Electron Devices*, vol. 60, no. 10, pp. 3216–3222, Oct. 2013.

[12] *TCAD Sentaurus Device Manual*, Synopsys, Inc., Mountain View, CA, USA, Mar. 2010.

[13] (2013, Oct. 10). *[i-MOS] e-HEMT: Surface-Potential-Based AlGaN HEMT Model* [Online]. Available: http://i-mos.org

[14] J. H. Davies, *The Physics of Low-Dimensional Semiconductors—An Introduction*, vol. 1. Cambridge, U.K.: Cambridge Univ. Press, 1998.

[15] J. Brews, "A charge-sheet model of the MOSFET," *Solid-State Electron.*, vol. 21, no. 2, pp. 345–355, 1978.

[16] P. Bendix, P. Rakers, P. Wagh, L. Lemaitre, W. Grabinski, C. C. Mcandrew, *et al.*, "RF distortion analysis with compact MOSFET models," in *Proc. IEEE CICC*, Oct. 2004, pp. 9–12.

[17] K. Joardar, K. K. Gullapalli, C. C. McAndrew, M. E. Burnham, and A. Wild, "An improved MOSFET model for circuit simulation," *IEEE Trans. Electron Devices*, vol. 45, no. 1, pp. 134–148, Jan. 1998.

[18] G. Gildenblat, X. Li, W. Wu, H. Wang, A. Jha, R. V. Langevelde, *et al.*, "PSP: An advanced surface-potential-based MOSFET model for circuit simulation," *IEEE Trans. Electron Devices*, vol. 53, no. 9, pp. 1979–1993, Sep. 2006.

[19] D. Ward and R. Dutton, "A charge-oriented model for MOS transistor capacitances," *IEEE J. Solid-State Circuits*, vol. 13, no. 5, pp. 703–708, Oct. 1978.

[20] R. Vetury, N. Q. Zhang, S. Keller, and U. K. Mishra, "The impact of surface states on the DC and RF characteristics of AlGaN/GaN HFETs," *IEEE Trans. Electron Devices*, vol. 48, no. 3, pp. 560–566, Mar. 2001.

[21] A. Koudymov, M. S. Shur, and G. Simin, "Compact model of current collapse in heterostructure field-effect transistors," *IEEE Electron Device Lett.*, vol. 28, no. 5, pp. 332–335, May 2007.
[22] A. Bansal, B. C. Paul, and K. Roy, "Modeling and optimization of fringe capacitance of nanoscale DGMOS devices," *IEEE Trans. Electron Devices*, vol. 52, no. 2, pp. 256–262, Feb. 2005.
[23] F. Pregaldiny, C. Lallement, and D. Mathiot, "A simple efficient model of parasitic capacitances of deep-submicron LDD MOSFETs," *Solid State Electron.*, vol. 46, no. 12, pp. 2191–2198, Dec. 2002.
[24] S. E. Laux, "Techniques for small-signal analysis of semiconductor devices," *IEEE Trans. Electron Device*, vol. 32, no. 10, pp. 2028–2037, Oct. 1985.
[25] (2013, Sep. 15). *COMSOL MultiPhysics User's Manual* [Online]. Available: http://www.comsol.com/products
[26] Z. Liu, G. I. Ng, S. Arulkumaran, Y. K. T. Maung, K. L. Teo, S. C. Foo, *et al.*, "Comprehensive study on the bias-dependent equivalent-circuit elements affected by PECVD SiN passivation in AlGaN/GaN HEMTs," *IEEE Trans. Electron Devices*, vol. 58, no. 2, pp. 473–479, Feb. 2011.
[27] Z. Tang, S. Huang, Q. Jiang, S. Liu, C. Liu, and K. J. Chen, "High-voltage (600- V) low-leakage low-current-collapse AlGaN/GaN HEMTs with AlN/SiN_x passivation," *IEEE Electron Device Lett.*, vol. 34, no. 3, pp. 366–368, Mar. 2013.
[28] J. Liu, Y. Zhou, J. Zhu, Y. Cai, K. M. Lau, and K. J. Chen, "DC and RF characteristics of AlGaN/GaN/InGaN/GaN double-heterojunction HEMTs," *IEEE Trans. Electron Devices*, vol. 54, no. 1, pp. 2–10, Jan. 2007.

Aixi Zhang (S'13) is currently pursuing the M.Phil. degree with the Hong Kong University of Science and Technology, Kowloon, Hong Kong.

His current research interests include the compact modeling and simulation of nanoelectronic devices.

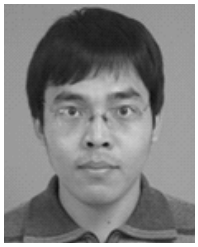

Lining Zhang (S'09–M'13) received the Ph.D. degree from the Hong Kong University of Science and Technology (HKUST), Hong Kong, in 2013.

He is currently a Research Associate with HKUST, and a Project Manager of *i*-MOS.

Zhikai Tang (S'10) received the B.S. degree from the University of Electronic Science and Technology of China, Chengdu, China. He is currently pursuing the Ph.D. degree with the Department of Electronic and Computer Engineering, The Hong Kong University of Science and Technology, Hong Kong.

Xiaoxu Cheng, photograph and biography not available at the time of publication.

Yan Wang, photograph and biography not available at the time of publication.

Kevin J. Chen (M'96–SM'06–F'14) received the B.S. degree from Peking University, Beijing, China, and the Ph.D. degree from the University of Maryland, College Park, MD, USA.

He is currently a Professor with the Department of Electronic and Computer Engineering, Hong Kong University of Science and Technology, Hong Kong.

Mansun Chan (S'92–M'95–SM'01–F'13) received the Ph.D. degree from the University of California at Berkeley, Berkeley, CA, USA, in 1995.

He has been with the Faculty of Electrical and Computer Engineering, Hong Kong University of Science and Technology, Hong Kong, since 1996.